Supporting Information for "Seismic attenuation tomography of Eastern Europe from ambient seismic noise analysis"

F. Borleanu [(1)], L. Petrescu[(1)], A.O. Placinta[(1)], F. Magrini[(2,3)], B. Grecu[(1)], M. Radulian[(1,4,5)], L. De Siena[(2,6)]

[1]National Institute for Earth Physics, Ilfov, Romania

[2]Institute of Geosciences, Geophysics and Geodynamics, Johannes Gutenberg University, Mainz, Germany

[3]Research School of Earth Sciences, Australian National University, Canberra, Australia

[4]Academy of Romanian Scientists, Bucharest, Romania

[5]Romanian Academy, Bucharest, Romania

[6]Dipartimento di Fisica e Astronomia (DIFA), Alma Mater Studiorum Università di Bologna, Bologna, Italy

The contents of this file: Figures S1 to S7

Fig. S1 is intended to supplement the manuscript's *Data and methods (IV)* section by displaying examples of estimated Rayleigh wave Green's functions (bandpass filtered between 5 and 10s, respectively between 10 and 20s) for paths between VOIR and the stations, placed up 500 km away.

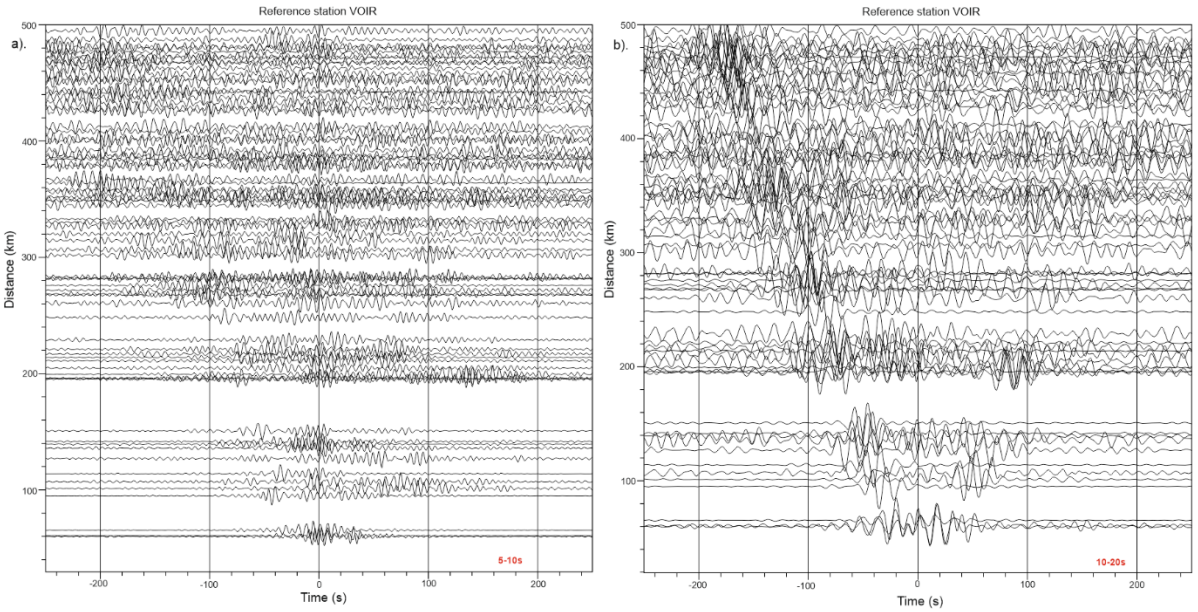

Figure S1. a) Example of estimated Rayleigh wave Green's functions (acausal and causal sections) in, **a)** 5-10s and **b)** 10-20s, for paths between VOIR and the stations, placed up 500 km away.

Fig. S2 is intended to supplement the manuscript's *Data and methods (IV)* section by displaying examples of several EGF's computed for different pairs of stations and their envelopes (bandpass filtered in various period ranges, given in red in the upper right corners) indicating the decay of the coda waves in time.

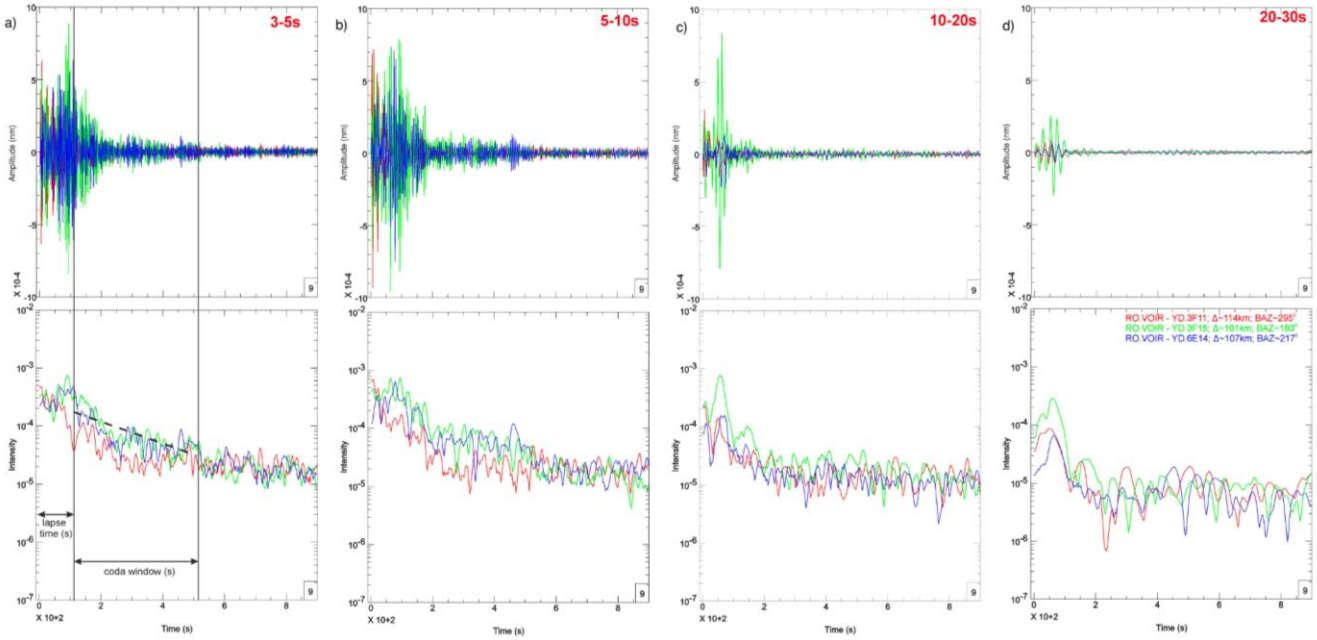

Figure S2. Examples of cross-correlograms (top) computed between different pairs of stations (in Romania, Fig. 3d) and their envelopes (bottom), indicating decay of the coda waves in time, bandpass filtered in the following period ranges: a) 3-5s; b) 5-10s; c) 10-20s; d) 20-30s. Vertical black lines delimit the coda window and lapse time, while the dashed black line displays the slope for envelope decay. The station pairs are shown in the upper right corner of the bottom plot of Figure S2d)

Fig. S3 is intended to supplement the manuscript's *Data and methods (IV)* and *Results (V)* sections by displaying the Qc dependence on backazimuth (in 5-10s) for various intervals of insterstation distances.

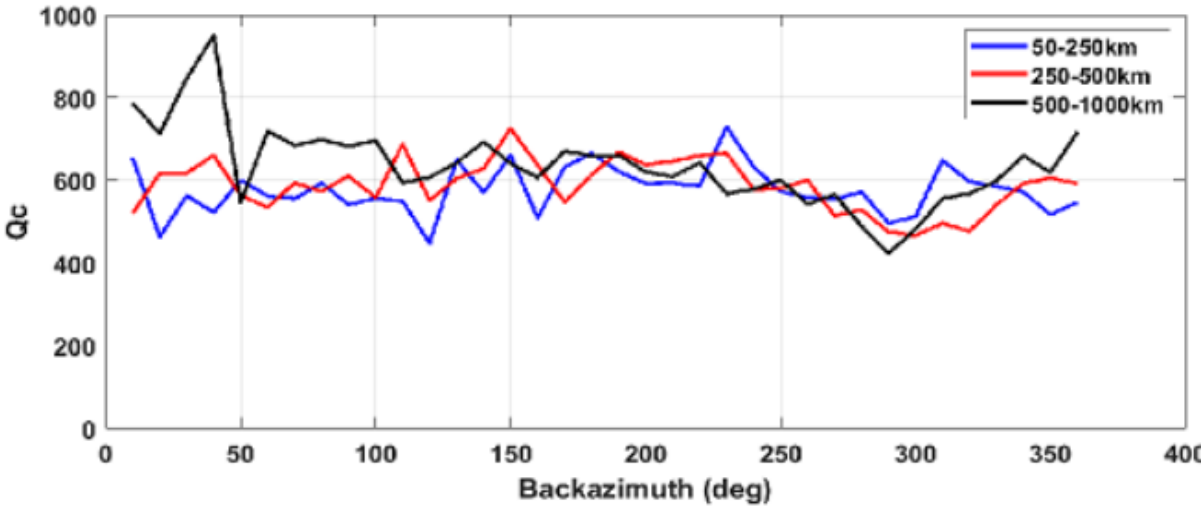

Figure S3. Qc in 5-10 s period range as a function of backazimuth at distances of 50-250 km, 250-500 km, and 500-1000 km

Fig. S4 is intended to supplement the manuscript's *Data and methods (IV)* and *Results (V)* sections by displaying the Qc dependence on travel time.

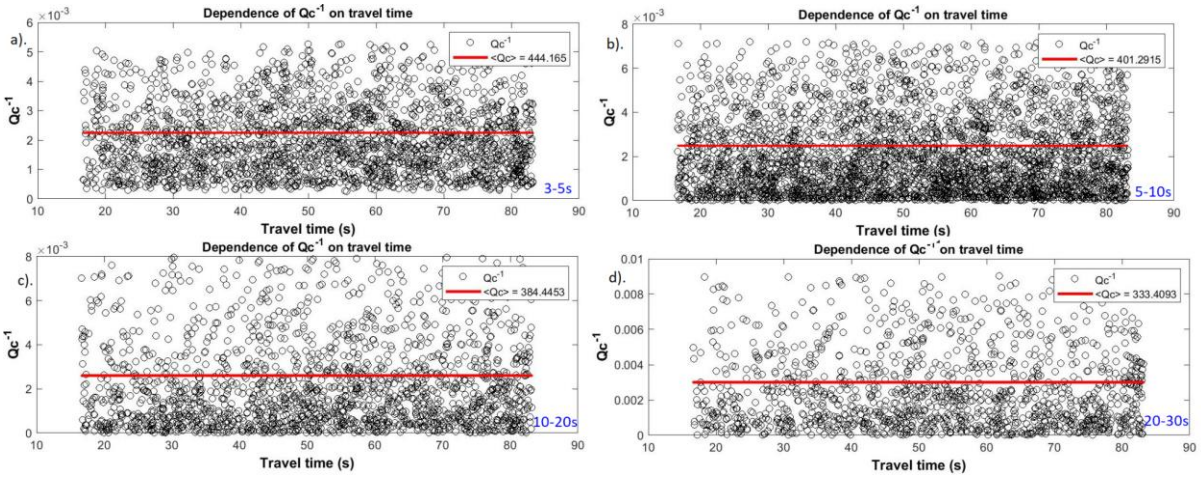

Figure S4. Inverse Qc dependence on travel time for a) 3-5s, b) 5-10s, c) 10-20s, d) 20-30s

Fig. S5 is intended to supplement the manuscript's *Data and methods (IV) and Results (V)* sections by displaying the number of correlations as a function of interstation distance and backazimuth.

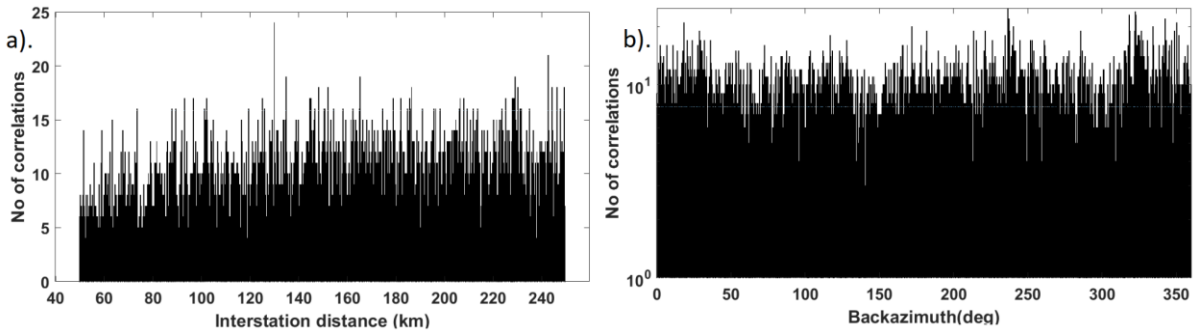

Figure S5. Number of correlations as a function of: a) interstation distance and b) backazimuth

Fig. S6 is intended to supplement the manuscript's *Data and methods (IV)* section by displaying the Qc sensitivity between source and receiver.

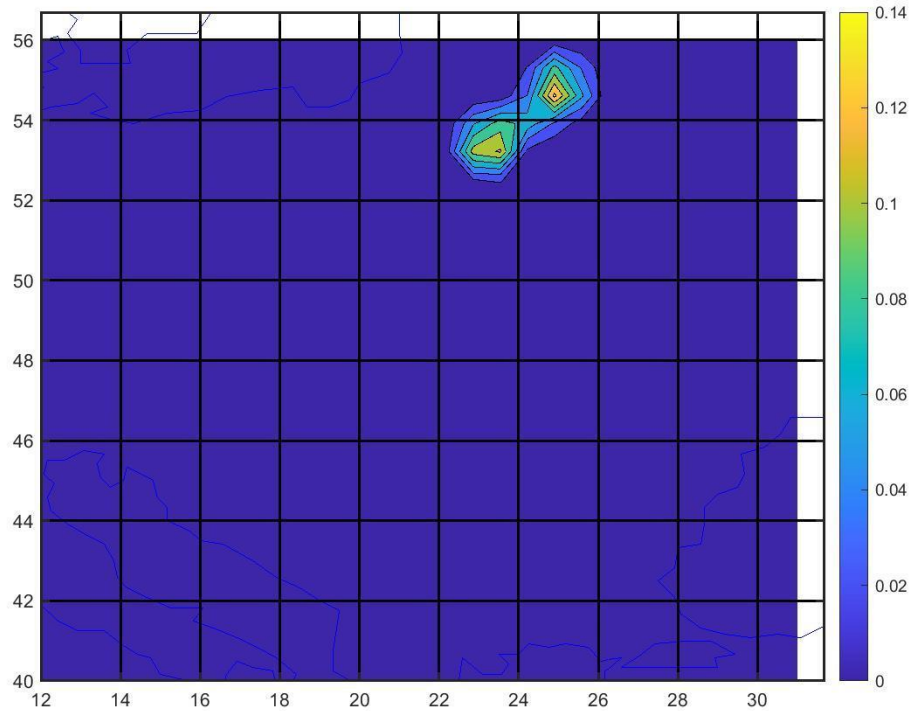

Figure S6. Qc sensitivity computed for 5-10s period range between a source (station PA82 of 7E network) and a receiver (station PF47 of 7E network)

Fig. S7 is meant to enrich the *Data and methods (IV) and Results (V)* sections by presenting the final ray path coverage resulting from the inversion algorithm.

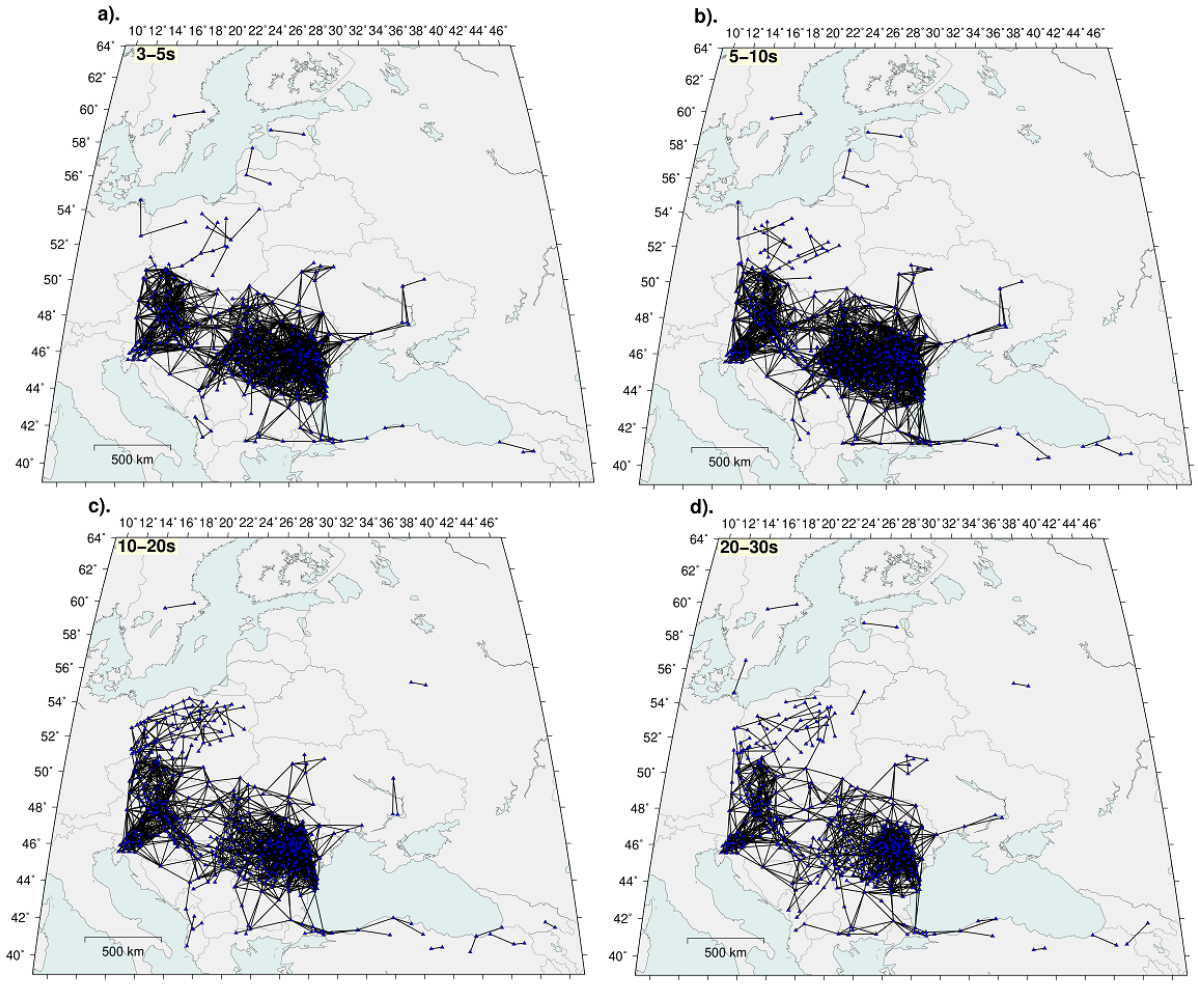

Figure S7. The final ray path coverage as resulted from the inversion algorithm in each of the period ranges a)3-5s; b)5-10s; c)10-20s; d)20-30s